16TH EUROPEAN CONFERENCE ON EARTHQUAKE ENGINEERING THESSALONIKI 18 - 21 JUNE 2018

MULTI-OBJECTIVE OPTIMAL DESIGN OF THE TUNED-MASS-DAMPER-INERTER (TMDI) FOR STOCHASTICALLY SUPPORT EXCITED BUILDING STRUCTURES

Alexandros TAFLANIDIS[1], Agathoklis GIARALIS[2]

ABSTRACT

The multi-objective optimal design is considered of tuned-mass-damper-inerter (TMDI) equipped linear building frames subject to seismic excitations modeled as stationary colored random processes. The TMDI couples the traditional tuned mass-damper (TMD) with an inerter. The latter is a two-terminal mechanical device developing a resisting force proportional to the relative acceleration of its terminals by the "inertance" constant. Previous work has shown that TMDI with large inertance can outperform the classical TMD for the same attached mass, if properly tuned/designed. This performance enhancement comes, though, at the expense of increased inerter forces that need to be accommodated by the host structure. A multi-objective design framework is considered to investigate the compromise between these two competing objectives. The first objective, representing the vibration suppression efficiency, is defined using first-passage reliability criteria, considering outcrossing of failure modes related to floor accelerations, inter-storey drifts, and attached mass displacement. A linear combination of the probabilities related to these modes is taken as objective function, following current performance-based seismic design practices. The second objective, representing the strengthening of the host structure required to accommodate the TMDI forces, corresponds to the stationary inerter force. A variant of the optimization problem is also considered by adopting as secondary objective the maximum force of either the inerter or the damper utilized in the TMDI configuration. In the illustrative example different topological configurations are examined for the TMDI. Results demonstrate that the proposed framework supports a comprehensive understanding of how the TMDI design establishes a compromise between the aforementioned objectives. Connection of the inerter at a lower floor than the one immediately below the TMDI mass can lead to significant reduction of both objectives.

Keywords: tuned mass-damper-inerter; multi-objective design; first-passage reliability; stationary response; peak inerter force

1. INTRODUCTION

Over the past several decades, the concept of the tuned mass-damper (TMD) has been extensively used for passive vibration suppression of dynamically excited structural systems (Chang 1999; Hoang et al. 2008). In its classical form, the TMD comprises a mass attached to the structure whose vibration motion is to be controlled (primary structure) via optimally designed/"tuned" linear spring and viscous damper (dashpot) elements. The effectiveness of the TMD depends heavily on its inertia property. In this context, recently a generalization of the classical TMD has been proposed by the second author (Marian and Giaralis 2013; Marian and Giaralis 2014) incorporating an "inerter" device: the tuned mass-damper-inerter (TMDI) [shown in Figure 1]. The inerter is a two-terminal device developing a resisting force proportional to the relative acceleration of its terminals (Smith 2002). The underlying constant of proportionality ("inertance") can be orders of magnitude larger than the physical mass of the inerter. In a number of studies (Marian and Giaralis 2013; Marian and Giaralis 2014; Giaralis and Petrini 2017) the TMDI has been shown to outperform the TMD, especially when smaller attached masses are examined. Beyond this mass amplification effect, an important aspect for TMDI

[1]Associate Professor, University of Notre Dame, Notre Dame, U.S.A, a.taflanidis@nd.edu
[2]Senior Lecturer, City, University of London, London, U.K., Agathoklis.Giaralis.1@city.ac.uk

applications (Giaralis and Taflanidis 2017) is the ability to influence the dynamics of the primary structure in a wide frequency range and not only at frequencies close to the own TMDI oscillation frequency, as is the case of the classical TMD. Another such aspect is the significant impact the TMDI topological configuration may have on the overall performance; it was shown in (Giaralis and Taflanidis 2017) that configurations with the inerter connecting to a lower floor than the floor immediately below the attached mass are more advantageous [see also (Giaralis and Petrini 2017)].

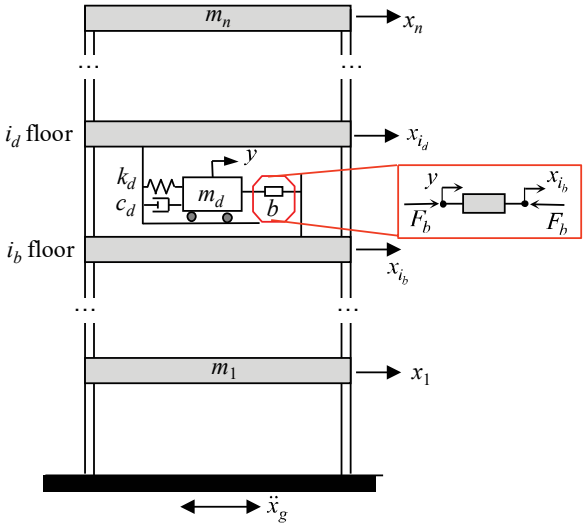

Figure 1. Tuned mass-damper-inerter (TMDI) equipped multi-storey frame structure.

This performance enhancement offered by the TMDI comes, though, at the expense of increased inerter forces that are transferred to the host structure (Giaralis and Petrini 2017). In this respect, this paper pursues optimal TMDI design for stochastically excited structures within a multi-objective setting that explicitly considers the compromise between the competing objectives of suppressing vibrations and avoiding large inerter forces. Linear damped primary structures are considered base-excited by filtered stationary white noise representing the seismic input action. The design variables include the inertance and the attached mass as well as the TMDI linear spring and viscous damper constants, whereas different topologies are examined with respect to the TMDI configuration. The first objective, representing the vibration suppression, is defined using first-passage reliability criteria, considering outcrossing of failure modes related to floor accelerations, inter-storey drifts, and attached mass displacement. A linear combination of the probabilities related to these modes is taken as objective function, following current performance-based seismic design practices. The second objective, representing the strengthening of the host structure required to accommodate the TMDI forces, corresponds to the stationary inerter force. A variant of the optimization problem is also considered by adopting as secondary objective the maximum force of either the inerter or the damper utilized in the TMDI configuration.

The governing equations of motion for a structure equipped with a TMDI are reviewed in the next section, followed (Section 3) by the stationary response statistics calculation and (Section 4) the multi-objective design problem formulation. Section 5 presents a case study for a TMDI equipped building frame exposed to stochastic seismic excitation. Concluding remarks are discussed in Section 6.

2. FORMULATION OF EQUATIONS OF MOTION

Consider the planar n-storey frame building, shown in Figure 1, whose oscillatory motion due to a ground acceleration $\ddot{x}_g$ is to be suppressed (primary structure). The TMDI consists of a classical linear passive tuned mass-damper (TMD) located at the i_d-th floor of the primary structure comprising a

mass m_d attached to the structure via a linear spring of stiffness k_d and a linear dashpot of damping coefficient c_d. The TMD mass is linked to the i_b-th floor by an inerter with inertance b. Let $\mathbf{x}_s \in \Re^n$ be the vector of floor displacements of the primary structure relative to the ground and $\ddot{x}_g \in \Re$ be the ground acceleration. Denote by $\mathbf{R}_d \in \Re^n$ the *TMD location* vector specifying the floor the TMD is attached to (i.e., vector of zeros with a single one in its i_d entry), and by $\mathbf{R}_b \in \Re^n$ be the *inerter location* vector specifying the floor the inerter is connected to (i.e., vector of zeros with a single one in its i_b entry). Let, also, $y \in \Re$ be the displacement of the TMD mass relative to the i_d floor and define the *connectivity* vector by $\mathbf{R}_c$=$\mathbf{R}_d$-$\mathbf{R}_b$. Then, the resisting inerter force, denoted by F_b in Figure 1, is equal to $F_b(t) = b\left[\ddot{y}(t) + \mathbf{R}_c\ddot{\mathbf{x}}_s(t)\right]$ and the coupled equations of motion become

$$\left(\mathbf{M}_s + \mathbf{R}_d m_d \mathbf{R}_d^T + \mathbf{R}_c b \mathbf{R}_c^T\right)\ddot{\mathbf{x}}_s(t) + \left(m_d \mathbf{R}_d + b\mathbf{R}_c\right)\ddot{y}(t) + \mathbf{C}_s\dot{\mathbf{x}}_s(t) + \mathbf{K}_s\mathbf{x}_s(t) = -\left(\mathbf{M}_s + \mathbf{R}_d m_d \mathbf{R}_d^T\right)\mathbf{R}_s\ddot{x}_g(t) \quad (1)$$

$$(m_d + b)\ddot{y}(t) + \left(m_d\mathbf{R}_d^T + b\mathbf{R}_c^T\right)\ddot{\mathbf{x}}_s(t) + c_d\dot{y}(t) + k_d y(t) = -m_d\mathbf{R}_d^T\mathbf{R}_s\ddot{x}_g(t)\ , \quad (2)$$

where $\mathbf{M}_s \in \Re^{nxn}$, $\mathbf{C}_s \in \Re^{nxn}$, and $\mathbf{K}_s \in \Re^{nxn}$ are the mass, damping, and stiffness matrices of the primary structure, respectively, and $\mathbf{R}_s \in \Re^n$ is the earthquake influence coefficient vector (vector of ones). Equation (2) suggests that the total inertia of the TMDI is equal to (m_d+b). Hence, the TMDI frequency ratio f_d, damping ratio ζ_d, inertance ratio β, and mass ratio μ are defined as

$$f_d = \sqrt{\frac{k_d}{(m_d + b)}} / \omega_1; \quad \zeta_d = \frac{c_d}{2(m_d + b)\omega_d}; \quad \beta = \frac{b}{M}; \quad \mu = \frac{m_d}{M}, \quad (3)$$

where ω_1 and M are the fundamental natural frequency and the total mass of the primary structure, respectively and $\omega_d = f_d\omega_1$ represents the TMDI natural frequency.

3. STATIONARY RESPONSE STATISTICS CALCULATION

Let $\ddot{x}_g$ be modeled as a stationary filtered Gaussian white noise stochastic process. A state-space formulation is utilized to determine the response characteristics required in the solution of the optimum TMDI design problem. In this setting, the excitation model is given by

$$\dot{\mathbf{x}}_q(t) = \mathbf{A}_q\mathbf{x}_q(t) + \mathbf{E}_q w(\mathrm{t}); \quad \ddot{x}_g(t) = \mathbf{C}_q\mathbf{x}_q(t)\ , \quad (4)$$

where $w(t) \in \Re$ is a zero-mean Gaussian white-noise process with spectral intensity equal to S_w=1/(2π); $\mathbf{x}_q(t) \in \Re^{n_q}$ is the state vector for the excitation; $\mathbf{A}_q \in \Re^{n_q x n_q}$, $\mathbf{E}_q \in \Re^{n_q x 1}$ and $\mathbf{C}_q \in \Re^{1 x n_q}$ are the state-space excitation matrices. Combining excitation model of Equation (4) with the equations of motion of the structural system in Equations (1) and (2) provides the augmented state-space system

$$\dot{\mathbf{x}}(t) = \mathbf{A}(\boldsymbol{\varphi})\mathbf{x}(t) + \mathbf{E}(\boldsymbol{\varphi})w(t); \ \ \mathbf{z}(t) = \mathbf{C}(\boldsymbol{\varphi})\mathbf{x}(t)\ , \quad (5)$$

where $\mathbf{x}(t) \in \Re^{n_x}$ is the state vector with n_x=2n+2+n_q; $\mathbf{z}(t) \in \Re^{n_z}$ is the vector of performance variables (response output of the system) with z_i denoting the i^{th} output; and $\mathbf{A}(\boldsymbol{\varphi})$, $\mathbf{E}(\boldsymbol{\varphi})$, $\mathbf{C}(\boldsymbol{\varphi})$ are the state-space matrices that are a function of vector $\boldsymbol{\varphi}$, which represents the controllable parameters of the TMDI system (μ, β, f_d and ζ_d). Note that the proposed formulation takes into account the spectral characteristics of the stochastic excitation, by appropriate augmentation of the state equation (Taflanidis and Scruggs 2010). This allows for an efficient calculation of the response statistics for the augmented system. The derivation of the state space matrices is discussed in the Appendix.

3.1 Basic stationary response statistics

Under the modelling assumptions discussed above, the output of the system, $\mathbf{z}(t)$, has a Gaussian distribution with zero mean and covariance matrix in stationary response given as

$$\mathbf{K}_{\mathbf{zz}} = \mathbf{C}(\boldsymbol{\varphi})\mathbf{P}(\boldsymbol{\varphi})\mathbf{C}(\boldsymbol{\varphi})^T;\ \mathbf{A}(\boldsymbol{\varphi})\mathbf{P}(\boldsymbol{\varphi}) + \mathbf{P}(\boldsymbol{\varphi})\mathbf{A}(\boldsymbol{\varphi})^T + \mathbf{E}(\boldsymbol{\varphi})\mathbf{E}(\boldsymbol{\varphi})^{\mathrm{T}} = 0\,, \tag{6}$$

where $\mathbf{P}(\boldsymbol{\varphi})$ corresponds to the state covariance matrix, obtained, as shown above, by the solution of an algebraic Lyapunov equation (Lutes and Sarkani 1997). The variance of each of the n_z system output variables $z_i = \mathbf{n}_i^T\mathbf{z}$ (i=1,2,…,n_z) and of their first time derivatives, needed later in evaluating the out-crosssing rate for z_i, are given, respectively, by

$$\sigma_{z_i}^2 = \mathbf{n}_i^T\mathbf{C}(\boldsymbol{\varphi})\mathbf{P}(\boldsymbol{\varphi})\mathbf{C}(\boldsymbol{\varphi})^T\mathbf{n}_i\,, \tag{7}$$

$$\sigma_{\dot{z}_i}^2 = \mathbf{n}_{z_i}^T\mathbf{C}(\boldsymbol{\varphi})\mathbf{A}(\boldsymbol{\varphi})\mathbf{P}(\boldsymbol{\varphi})\mathbf{A}(\boldsymbol{\varphi})^T\mathbf{C}(\boldsymbol{\varphi})^T\mathbf{n}_{z_i}\,, \tag{8}$$

where $\mathbf{n}_i$ is a n_z dimensional vector with zeros with the i_{th} component being one. In deriving the expression for the derivatives in Equation (8) the relationship $\mathbf{C}(\boldsymbol{\varphi})\mathbf{E}(\boldsymbol{\varphi}) = 0$ is assumed to hold. The latter condition is necessary to ensure that the out-crossing rate of the z_i stochastic process is finite (Taflanidis and Scruggs 2010). Lastly, the frequency response function of z_i, also required in the calculation of the out-crossing rate of z_i, is given by

$$\mathbf{H}_{z_i}(\omega;\boldsymbol{\varphi}) = \mathbf{n}_i^T\mathbf{C}(\boldsymbol{\varphi})[i\omega\mathbf{I} - \mathbf{A}(\boldsymbol{\varphi})]^{-1}\mathbf{E}(\boldsymbol{\varphi})\,. \tag{9}$$

3.2 First-passage failure probability

The design framework discussed in the next section utilizes the probability that an output (performance) variable z_i exceeds a given threshold β_i (defining acceptable performance) within some time-window T of the excitation (strong ground motion duration). This probability is expressed as

$$P_i(\boldsymbol{\varphi}\,|\,\beta_i, T) = P\Big[\big|z_i(\tau)\big| > \beta_i \text{ for some } \tau \in [0,T]\Big], \tag{10}$$

and may be calculated as the first-passage probability for output z_i out-crossing threshold β_i. Under the stationarity assumption, the considered probability is approximated by (Taflanidis and Beck 2006)

$$P_i(\boldsymbol{\varphi}\,|\,\beta_i, T) = 1 - \mathrm{e}^{-\nu_i^+(\boldsymbol{\varphi})T};\ \ \nu_i^+(\boldsymbol{\varphi}) = \lambda_i(\boldsymbol{\varphi})r_i^+(\boldsymbol{\varphi})\,, \tag{11}$$

where $\nu_i^+(\boldsymbol{\varphi})$ is the conditional out-crossing rate for z_i, which, as shown above, is a product of two factors, Rice's unconditional out-crossing rate $r_i^+(\boldsymbol{\varphi})$ (Rice 1944, 1945), and the temporal-correlation correction factor $\lambda_i(\boldsymbol{\varphi})$, introduced as a heuristic "correction factor" to address correlation between out-crossing events (Lutes and Sarkani 1997). The former is given by

$$r_i^+(\boldsymbol{\varphi}\,|\,\boldsymbol{\theta}) = \frac{\sigma_{\dot{z}_i}(\boldsymbol{\varphi}\,|\,\boldsymbol{\theta})}{\pi\sigma_{z_i}(\boldsymbol{\varphi}\,|\,\boldsymbol{\theta})}\mathrm{e}^{-\frac{\beta_i^2}{2\sigma_{z_i}^2(\boldsymbol{\varphi}|\boldsymbol{\theta})}}, \tag{12}$$

whereas for the latter the correction factor proposed by Taflanidis and Beck (2006) is utilized here,

$$\lambda_i(\boldsymbol{\varphi}) \approx \frac{1 - \exp\left\{-q(\boldsymbol{\varphi})^{0.6}\left(\frac{2}{\sqrt{\pi}}\right)^{0.1}\frac{\beta_i\sqrt{2}}{\sigma_{z_i}(\boldsymbol{\varphi})}\right\}}{1 - \exp\left\{-\frac{\beta_i^2}{2\sigma_{z_i}^2(\boldsymbol{\varphi})}\right\}};\ q(\boldsymbol{\varphi}) = \frac{\sigma_{z_i}^6(\boldsymbol{\varphi})}{4\pi\int_{-\infty}^{\infty}|\omega|S_{z_iz_i}(\omega\,|\,\boldsymbol{\varphi})d\omega\int_{-\infty}^{\infty}S_{z_iz_i}^2(\omega\,|\,\boldsymbol{\varphi})d\omega}, \tag{13}$$

where $S_{z_iz_i}(\omega\,|\,\boldsymbol{\varphi})$ is the spectral density function for z_i. The stationary variances needed in Equaitons

(12) and (13) are provided through Equations (7) and (8), whereas for calculation of the one-dimensional integrals in the denominator of $q(\boldsymbol{\varphi})$ the spectral density $S_{z_i z_i}(\omega \mid \boldsymbol{\varphi})$ is substituted by

$$S_{z_i z_i}(\omega \mid \boldsymbol{\varphi}) = S_w \left| H_{z_i}(\omega \mid \boldsymbol{\varphi}) \right|^2 \tag{14}$$

with $H_{z_i}(\omega \mid \boldsymbol{\varphi}, \boldsymbol{\theta})$ given by Equation (9). The frequency range over which the system dynamics are important is partitioned at desired points and the frequency response is calculated. Each one-dimensional integral is then evaluated via standard numerical integration.

4. MULTI-OBJECTIVE DESIGN FRAMEWORK

4.1 Performance objectives selection and multi-objective design problem formulation

The first objective, representing the vibration suppression efficiency of the TMDI applications, is defined, similarly to (Giaralis and Taflanidis 2017), as the consequences related to the different failure modes. Each of these modes is defined through some specific response output z_i, representing the engineering demand parameter for that failure mode, and ultimately though probability $P_i(\boldsymbol{\varphi} \mid \beta_i, T)$, whose estimation was discussed in Section 3.2. Let $\mathbf{i}_f$ represent the index sets associated with the failure modes under consideration and n_f the total number of failure modes examined. Note that response vector $\mathbf{z}$ may contain additional response outputs, beyond the ones required for estimation of the occurrence probabilities of the different failure modes, in other words n_f is not necessarily equal to n_z. The first design objective corresponds to the combination of probabilities $P_i(\boldsymbol{\varphi} \mid \beta_i, T)$ over set $\mathbf{i}_f$

$$J_1(\boldsymbol{\varphi}) = \sum\nolimits_{i \in \mathbf{i}_f}^{n_f} w_i P_i(\boldsymbol{\varphi} \mid \beta_i, T), \tag{15}$$

where w_i are weights representing the relative consequences for each failure mode. Notably, this definition of $J_1(\boldsymbol{\varphi})$, which adds the contribution of each individual failure mode (upon weighting), is well aligned with the current performance based earthquake engineering practice of summing the contributions from all damage states (Goulet et al. 2007) in defining structural performance.

The second objective, representing the strengthening of the host structure required to accommodate the TMDI forces, corresponds to the inerter force. Since under the stated stationary assumptions the peak response for z_i can be related to its stationary variance $\sigma_{z_i}^2$ through the peak factor (Der Kiureghian 1980) which can be approximated as a constant, the standard deviation of the inerter force is taken, equivalently, as the second design objective. A variant of the optimization problem is also considered by adopting as second objective the maximum force of either the inerter or the damper utilized in the TMDI configuration. This variant is motivated by the fact that the damper forces connecting the TMDI to the host structure may become excessive, especially for large TMDI mass, so they should be considered in evaluating the strengthening needed for safe TMDI force transfer to the host structure. The second design objective is therefore defined as

$$J_2(\boldsymbol{\varphi}) = \sigma_{F_b} \quad \text{or} \quad J_2(\boldsymbol{\varphi}) = \max(\sigma_{F_b}, \sigma_{F_d}), \tag{16}$$

where σ_{F_b} and σ_{F_d} are the standard deviations of the inerter force $F_b(t)$ and damper force $F_d(t) = c_d \dot{y}(t)$, respectively. Both the objective functions in Equation (16) correspond to specific elements of σ_{z_i}, for an appropriate definition of the response vector as detailed in the Appendix. Therefore, they are readily available from Equation (7).

Lastly, a multi-objective design problem considering concurrently design objectives in Equations (15) and (16) is formulated as

$$\boldsymbol{\varphi}^* = \arg\min_{\boldsymbol{\varphi} \in \Phi} \left\{ J_1(\boldsymbol{\varphi}), J_2(\boldsymbol{\varphi}) \right\}^T, \tag{17}$$

where Φ represents the admissible design space. Since the two design objectives are competing there is no design configuration that simultaneously minimizes them both. The design optimization problem is transformed to identification of the *Pareto optimal* solutions, also known as dominant designs. A design configuration is Pareto optimal, denoted $\boldsymbol{\varphi}_p$, if there is no other configuration that improves one objective without detriment to the other. The set of all such configurations is denoted as the *Pareto set* $\boldsymbol{\Phi}_p$. *The Pareto front* is the representation of the Pareto set in the objective function space $\mathbf{J}_p = \{[J_1(\boldsymbol{\varphi})\ J_2(\boldsymbol{\varphi})] \,|\, \boldsymbol{\varphi} \in \boldsymbol{\Phi}_p\}$. It is generally impractical to find all Pareto optimums so the optimization strategies usually aim at finding a subset of them that represents $\mathbf{J}_p$ well and can provide the decision maker with a comprehensive picture of trade-offs (Zitzler et al. 2000). The multi-objective design problem facilitates ultimately the identification of a range of TMDI configurations (Pareto optimal solutions) striking a trade-off among (i) vibration suppression efficiency and (ii) strengthening required for accommodating TMDI force transfer to the host structure. The designer or decision maker (e.g. building owner) can ultimately make the final decision among the Pareto optimal solutions, incorporating any additional considerations including architectural constraints for the TMDI implementation.

4.2 Solution to multi-objective problem

The multi-objective optimization problem of Equation (17) is solved by the epsilon-constraint method (Haimes et al. 1971). This numerical optimization approach is preferred here due to its ability to discover nonconvex regions of the Pareto front (compared to, for example, the weighted sum approach) and the fact that it can provide a front with a pre-determined resolution (compared to, for example, evolutionary approaches). Objective $J_1(\boldsymbol{\varphi})$ is used as *optimization function* and objective $J_2(\boldsymbol{\varphi})$ as *constraint function*. The epsilon-constraint method converts the multi-objective optimization problem to a set of single-objective constraint optimization problems with different constraints ε^r

$$\begin{aligned} &\boldsymbol{\varphi}_p^r = \arg\min_{\boldsymbol{\varphi}\in\Phi}\ J_1(\boldsymbol{\varphi}) \\ &\text{such that } J_2(\boldsymbol{\varphi}) \le \varepsilon^r, \end{aligned} \tag{18}$$

where the superscript r is utilized to describe the rth such constraint. Systematic variation of ε^r facilitates identification of the Pareto front. The formulation of Equation (18) allows ultimately the identification of TMDI configurations that facilitate the optimum vibration suppression while maintaining the inerter forces below the target threshold of ε^r.

For deciding the range for ε^r the anchor point of the Pareto front corresponding to the maximum of $J_2(\boldsymbol{\varphi})$ is first obtained by solving of the unconstrained single objective-optimization

$$\boldsymbol{\varphi}_1^{an} = \arg\min_{\boldsymbol{\varphi}\in\Phi}\ J_1(\boldsymbol{\varphi}). \tag{19}$$

The maximum value for $J_2(\boldsymbol{\varphi})$ across the front is $J(\boldsymbol{\varphi}_1^{an})$. The minimum is obviously 0. The range for feasible epsilon constraints ε is therefore $[0\ J(\boldsymbol{\varphi}_1^{an})]$. If n_p equally spaced solutions are desired, then each ε^r is chosen as

$$\varepsilon^r = \frac{r}{n_p} J(\boldsymbol{\varphi}_1^{an});\ r = 1,...,n_p. \tag{20}$$

Evidently for $r=n_p$ the optimal configuration is $\boldsymbol{\varphi}_1^{an}$ whereas for $r=0$ (i.e. corresponding to the other anchor point of the front) the solution for the main formulation for $J_2(\boldsymbol{\varphi})$ is the TMD ($b=0$ and so $F_b(t)$ is minimized) that offers maximum vibration suppression, whereas for the variant formulation is the uncontrolled structure (no forces at all associated with the TMDI).

5. ILLUSTRATIVE NUMERICAL EXAMPLE

The design approach is illustrated by considering a 10-storey building frame (Figure 1) equipped with a single TMDI previously used in (Giaralis and Taflanidis 2017).

5.1 Structural and excitation models

The lumped mass per story is 900ton whereas the stiffness has a gradual decrease along height; it is 782.22MN/m for the bottom four stories, 626.10MN/m for the three intermediate ones and 469.57MN/m for the top three stories. Modal damping equal to 3.5% is considered. The natural periods the structure along with the participation factors in parenthesis are 1.5s (81.7%), 0.55s (11.8%), 0.33s (3.7%). The stationary seismic excitation $\ddot{x}_g$ is described by a high-pass filtered Kanai-Tajimi power spectrum (Clough and Penzien 1993)

$$S_g(\omega) = s_o \frac{\omega_g^4 + 4\zeta_g^2\omega^2\omega_g^2}{\left(\omega_g^2 - \omega^2\right)^2 + 4\zeta_g^2\omega_g^2\omega^2} \frac{\omega^4}{\left(\omega_f^2 - \omega^2\right)^2 + 4\zeta_f^2\omega_f^2\omega^2}. \tag{21}$$

In the above equation the Kanai-Tajimi parameters ω_g and ζ_g represent the stiffness/frequency and damping properties, respectively, of the supporting ground modeled by a linear damped SDOF oscillator driven by white noise. Further, the parameters ω_f and ζ_f control the cut-off frequency and the "steepness" of a high-pass filter used to suppress the low frequency content allowed by the Kanai-Tajimi filter. Lastly, s_o is chosen to achieve a desired pre-specified value for the root mean square acceleration a_{RMS} of the considered seismic input. For the purposes of this study, the adopted values are ω_g=3π, ζ_g=0.4, ω_f=π/2, ζ_f=0.8, a_{RMS}=0.062g.

The vector of engineering demand parameters for defining $J_1(\boldsymbol{\varphi})$ includes inter-storey drifts, associated with the structural integrity of the primary structure, and absolute floor accelerations, associated with the response of secondary equipment (building contents) housed by the primary structure, for all 10 floors, the TMD mass displacement, associated with the stroke of the damper and inerter and with the required clearance between the mass and the host structure (n_f= 21 performance variables in total). The assumed thresholds β_i are chosen as 3.3 cm for inter-storey drifts, 0.5g for floor accelerations, and 1m for the stroke (common for mass damper applications). Justification of the threshold selection is included in (Giaralis and Taflanidis 2017). Without loss of generality, equal weights w_i=1/n_z are considered for all performance variables. This assumes equal consequences for all failure modes and was chosen (see discussion in next paragraph) to provide a comparable contribution to the total failure probability from the drift and acceleration related failure modes. For the uncontrolled structure, the objective function $J_1(\boldsymbol{\varphi})$ is 12.38%. When considering only drift or acceleration responses this value becomes 10.94% or 13.83%, respectively. The response vector $\mathbf{z}$ includes, additionally, the inerter and damper forces, leading to n_z=23. The definition of the state-space output matrices for this choice of $\mathbf{z}$ is discussed in the Appendix. Since the response variables needed for the failure modes are ordered first, the index vector for the failure modes is $\mathbf{i}_f$=1, .., 21.

The vector of dimensionless TMDI design variables, $\boldsymbol{\varphi}$, includes the damping, frequency and inertance ratios, defined in Eq. (3), i.e., $\boldsymbol{\varphi}=[\zeta_d\ f_d\ \beta]^T$. The mass ratio μ is treated as a fixed pre-specified variable and a parametric investigation is undertaken for different values of μ ranging from 0.1% to 5% of the total structural mass. A number of different TMDI topologies are examined, i.e. different i_d and i_b floor pairs. Further, two different designs are examined with respect to the selection of $J_2(\boldsymbol{\varphi})$ in Equation (16). Primary design formulation, considering only the inerter force is denoted by D_1 whereas the variant, examining both the inerter and damper forces, is denoted by D_2.

5.1 Results and discussion

Results are shown in Figures (2) to (4). Figure 2 plots Pareto fronts for six different TMDI topological configuration and six different mass ratios for design problem D_1. Figure 3 shows the corresponding Pareto optimal values for design vector $\boldsymbol{\varphi}$ for three of these topological configurations. Finally, Figure 4 includes results for design problem D_2 for three topological configurations. In Figures 2 and 4 optimal TMD designs (obtained for β=0 for each mass ration) lie on the x-axis for which J_2=0. In Figure 3 these designs lie at the origin. For the Pareto front representation value of n_p is set to 22. Note, though, that the number of designs identified for some of the cases may not be n_p= 22. For example, for D_1 design, if the TMD (β=0 and therefore J_2 is minimized) outperforms TMDI for some specific ε_m^r value, then all solutions of the optimization of Equation (18) for $\varepsilon^r < \varepsilon_m^r$ correspond to the same optimal TMD configuration and, therefore, they do not yield different Pareto optimal configurations. For D_2 design the same argument holds with respect to the uncontrolled structure.

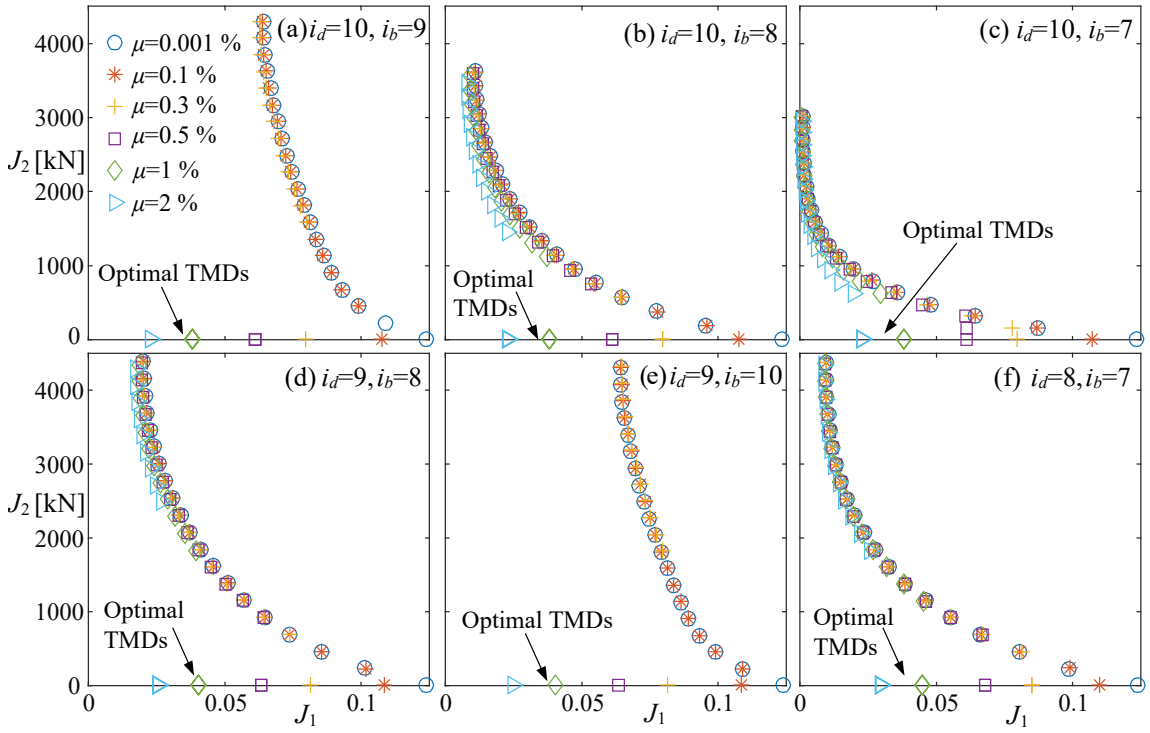

Figure 2. Pareto front for design problem D_1 for six different topological configurations for the TMDI implementation (sub-plots) and six different mass ratios masses (curves for each subplot).

The results demonstrate the usefulness and applicability of the proposed design framework to facilitate the identification of solutions with drastically different performance across the two examined objectives. As discussed in the introduction, the protection offered by the TMDI (J_1 values significantly reduced with respect to the uncontrolled structure) comes at the expense of significant forces exerted by the inerter to the host structure (large J_2 values). The multi-objective formulation allows identification of Pareto optimal configurations that establish a compromise between protection efficiency and inerter forces. Based on the threshold that is acceptable for this force for the specific application (or any other decision criterion) the final design configuration may be chosen among the identified Pareto optimal solutions. Comparison between Figures 2 and 4 shows that the damper force is significantly smaller than the inerter force and ultimately does not impact the design formulation; the only concern should be the safe inerter force transfer to the host structure. The inerter forces are primarily related to the β value as evident from the results in Figure 3; large variations exist for β across the front and evident correlation to the J_2 value.

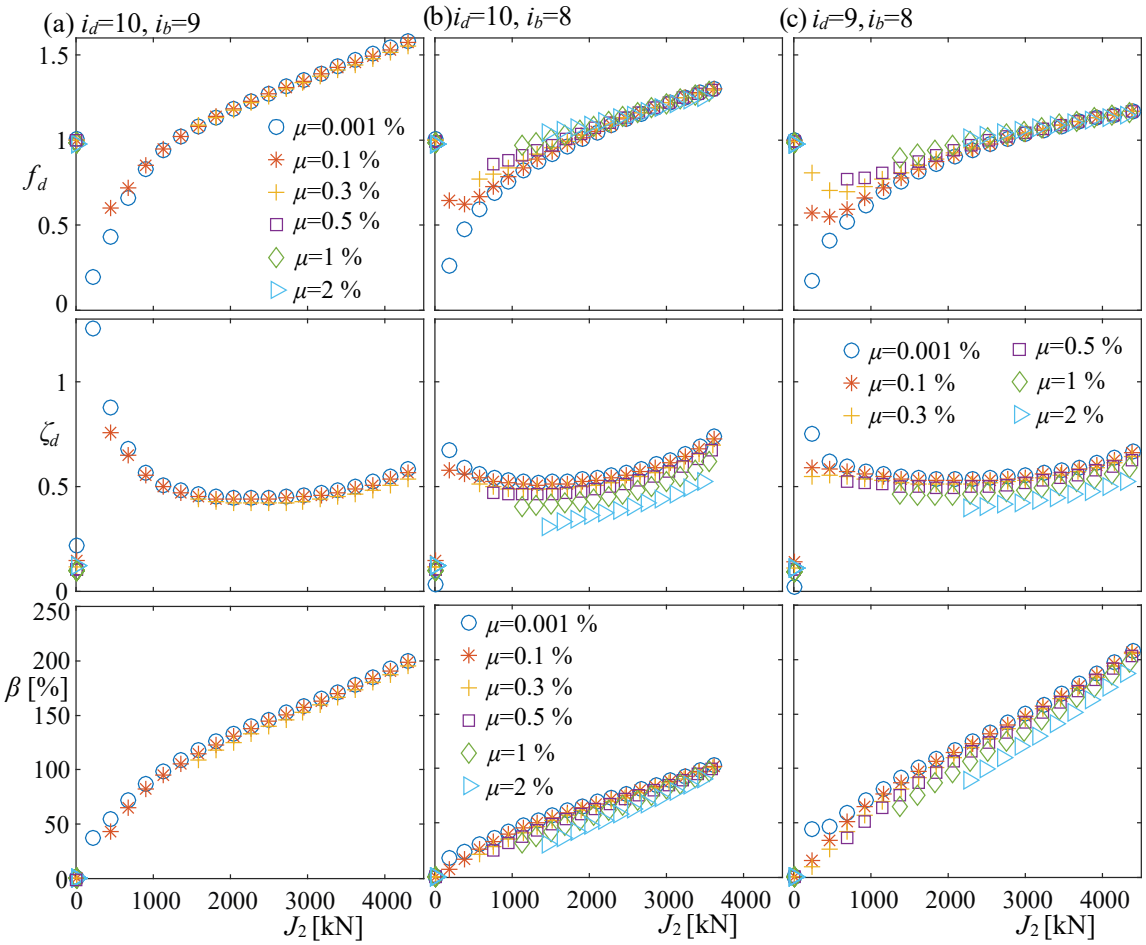

Figure 3. Optimal values for f_d, ζ_d and β along the Pareto front [design variables are plotted with respect to the corresponding value of J_2]. Rows corresponds to three different topological configurations. Curves in each subplot correspond to different mass ratios.

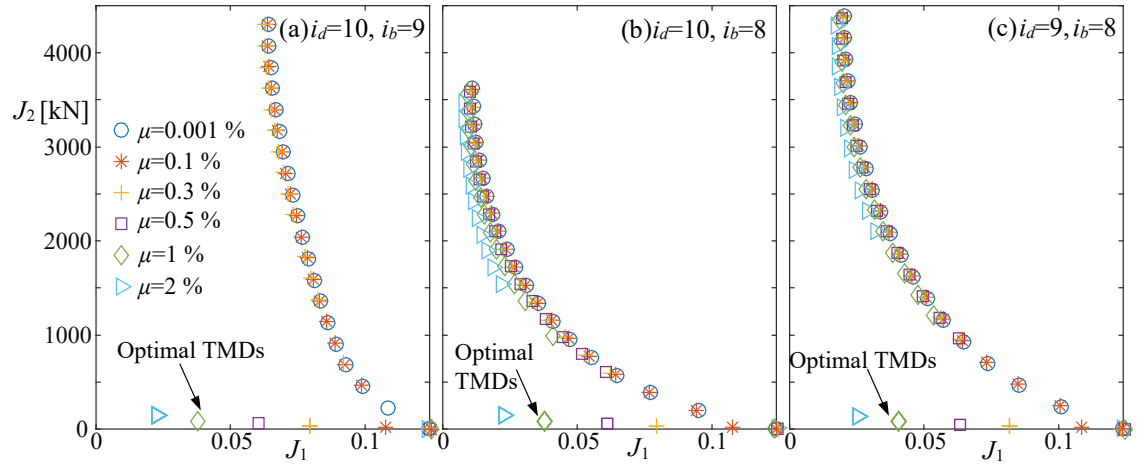

Figure 4. Pareto front for design problem D_2 for three different topological configurations for the TMDI implementation (sub-plots) and six different mass ratios masses (curves for each subplot)

With respect to the TMDI behavior for different mass ratios, variation of μ has small impact on the optimal performance across both objectives (Figures 2, 4) and on the optimal design configuration

(Figure 3) across the Pareto front up to the point that the TMD outperforms TMDI for a given μ. The latter creates a sharp jump of the Pareto front to the optimal TMD configuration. The insensitivity to μ agrees with the well-reported in the literature mass amplification effect endowed to the TMDI by the inerter (Marian and Giaralis 2013; Marian and Giaralis 2014; Giaralis and Petrini 2017). In general, larger masses tend to provide only marginally better TMDI performance, especially when the inerter force is constrained.

Connecting the inerter at a higher floor provides significant deterioration of the performance [compare parts (d) and (e) in Figure 2] and should be avoided as also shown in (Giaralis and Taflanidis 2017). Placement of the entire TMDI configuration at lower floors [compare parts (d), (f) to (a) in Figure 2] or connecting the inerter to a floor two [part (b) in Figure 2 or 4] or three [part (c) in Figure 2] stories below the i_d story provides greater protection efficiency. This agrees with the trends reported by Giaralis and Taflanidis (2017) and Giaralis and Petrini (2017). The interesting extension here is the investigation of the impact on the inerter force. Placement of the TMDI at a lower floor does not have a significant impact on the inerter forces. Note that the Pareto optimal β values [compare parts (a) and (c) in Figure 3] do not significantly change either. On the other hand, *configurations in which the inerter spans two or three stories offer considerable reduction with respect to the inerter forces* [note also the reduced β values in part (b) of Figure 3]. This new finding adds yet another advantage of connecting the inerter to the lowest floor possible subject to architectural constraints; not only greater protection efficiency is achieved (smaller J_1 values) but also a reduced demand is created with respect to the (generally significant) inerter forces transferred to the host structure (smaller J_2 values).

6. CONCLUSIONS

The multi-objective design of the tuned-mass-damper-inerter (TMDI) was considered in this study for seismic excitations modeled as stationary stochastic process. The objectives examined include both the protection efficiency as well as the forces that are exerted by the inerter on the host structure. The first objective, representing the vibration suppression, was defined using first-passage reliability criteria, considering outcrossing of failure modes related to floor accelerations, inter-storey drifts and attached mass displacement. A linear combination of the probabilities related to these modes was taken as objective function, following current performance-based seismic design practices. The second objective, representing the strengthening of the host structure required to accommodate the TMDI forces, was taken as the stationary inerter force. A variant of the optimization problem was also considered by adopting as secondary objective the maximum force of either the inerter or the damper utilized in the TMDI configuration. Linear structural model was considered and all required statistics (stationary response, first passage probabilities) were analytically obtained leveraging state-space formulation. For the solution of the multi-objective problem the epsilon constraint method was chosen due to its abilities to identify non-convex fronts and offer a evenly populated discrete representation of the front. Selection of the constraints was done by considering first the single-objective design for minimizing the vibration suppression. As case study an implementation to 10-storey frame was considered. Different topologies were examined with respect to the TMDI configuration. It was verified in the example that the inerter forces are significant, much larger than the damper forces, and that the proposed design formulation facilitates the identification of solutions with drastically different performance across the two examined objectives. Since the damper forces are smaller than the inerter ones their explicit consideration offers little practical interest. The main design variable changing across the Pareto front was found to be the inertance value. Finally it was shown that connection of the inerter to a floor lower than the one immediately underneath the TMDI mass offers significant benefits. Not only greater protection efficiency is achieved but also a reduced demand is created with respect to the inerter forces transferred to the host structure.

7. ACKNOWLEDGMENTS

The second author gratefully acknowledges the financial support by EPSRC in UK, under grant

EP/M017621/1.

8. REFERENCES

Chang, C. C. (1999). "Mass dampers and their optimal designs for building vibration control " *Engineering Structures*, 21, 454-463.

Clough, R. W., and Penzien, J. (1993). *Dynamics of structures*, McGraw-Hill Inc., New York, N.Y.

Der Kiureghian, A. (1980). "Structural response to stationary excitation." *Journal of Engineering Mechanics, ASCE*, 106((EM6)), 1195-1213.

Giaralis, A., and Petrini, F. (2017). "Wind-induced vibration mitigation in tall buildings using the tuned mass-damper-inerter." *Journal of Structural Engineering*, 143(9), 04017127.

Giaralis, A., and Taflanidis, A. (2017). "Optimal tuned mass-damper-inerter (TMDI) design for seismically excited MDOF structures with model uncertainties based on reliability criteria." *Structural Control and Health Monitoring*, DOI: 10.1002/stc.2082.

Goulet, C. A., Haselton, C. B., Mitrani-Reiser, J., Beck, J. L., Deierlein, G., Porter, K. A., and Stewart, J. P. (2007). "Evaluation of the seismic performance of code-conforming reinforced-concrete frame building-From seismic hazard to collapse safety and economic losses." *Earthquake Engineering and Structural Dynamics*, 36(13), 1973-1997.

Haimes, Y. Y., Ladson, L., and Wismer, D. A. (1971). "Bicriterion formulation of problems of integrated system identification and system optimization." *IEEE Transactions on Systems Man and Cybernetics*(3), 296-&.

Hoang, N., Fujino, Y., and Warnitchai, P. (2008). "Optimal tuned mass damper for seismic applications and practical design formulas." *Engineering Structures*, 30(3), 707-715.

Lutes, L. D., and Sarkani, S. (1997). *Stochastic analysis of structural and mechanical vibrations*, Prentice Hall, Upper Saddle River, NJ.

Marian, L., and Giaralis, A. (2013)."Optimal design of inerter devices combined with TMDs for vibration control of buildings exposed to stochastic seismic excitations." *11th International Conference on Structural Safety and Reliability*, June 16-20, New York, US, 1025-1032.

Marian, L., and Giaralis, A. (2014). "Optimal design of a novel tuned mass-damper-inerter (TMDI) passive vibration control configuration for stochastically support-excited structural systems." *Probabilistic Engineering Mechanics*, 38, 156-164.

Rice, S. O. (1944, 1945). "Mathematical analysis of random noise." *Bell System Technical Journal*, 23 and 24.

Smith, M. C. (2002). "Synthesis of mechanical networks: the inerter." *Automatic Control, IEEE Transactions on*, 47(10), 1648-1662.

Taflanidis, A. A., and Beck, J. L. (2006). "Analytical approximation for stationary reliability of certain and uncertain linear dynamic systems with higher dimensional output." *Earthquake Engineering and Structural Dynamics*, 35(10), 1247-1267.

Taflanidis, A. A., and Scruggs, J. T. (2010). "Performance measures and optimal design of linear structural systems under stochastic stationary excitation." *Structural Safety*, 32(5), 305-315.

Zitzler, E., Deb, K., and Thiele, L. (2000). "Comparison of multiobjective evolutionary algorithms: Empirical results." *Evolutionary computation*, 8(2), 173-195.

APPENDIX

The state-space representation of the TMDI-equipped *n*-story structure in Equations (1) and (2) reads

$$\dot{\mathbf{x}}_{ss}(t) = \mathbf{A}_s(\boldsymbol{\varphi})\mathbf{x}_{ss}(t) + \mathbf{E}_s(\boldsymbol{\varphi})\ddot{x}_g(t), \qquad \mathbf{z}(t) = \mathbf{C}_s(\boldsymbol{\varphi})\mathbf{x}_{ss}(t) \tag{22}$$

where $\mathbf{x}_{ss} \in \Re^{2n+2}$ is the state vector collecting relative to the ground displacements and velocities of all

stories and of the attached mass (relative to i_b floor), $\mathbf{x}_s = [\mathbf{x}_s^T \quad y \quad \dot{\mathbf{x}}_s^T \quad \dot{y}]^T$, and the matrices in Equation (22) are defined as

$$\mathbf{A}_s(\boldsymbol{\varphi}) = \begin{bmatrix} \mathbf{0}_{(n+1)\mathrm{x}(n+1)} & \mathbf{I}_{(n+1)} \\ -\mathbf{M}_t^{-1}(\boldsymbol{\varphi}) \begin{bmatrix} \mathbf{K}_s & \mathbf{0}_{n\mathrm{x}1} \\ \mathbf{0}_{1\mathrm{x}n} & k_d \end{bmatrix} & -\mathbf{M}_t^{-1}(\boldsymbol{\varphi}) \begin{bmatrix} \mathbf{C}_s & \mathbf{0}_{n\mathrm{x}1} \\ \mathbf{0}_{1\mathrm{x}n} & c_d \end{bmatrix} \end{bmatrix}; \; \mathbf{E}_s(\boldsymbol{\varphi}) = \begin{bmatrix} \mathbf{0}_{(n+1)\mathrm{x}1} \\ -\mathbf{M}_t^{-1}(\boldsymbol{\varphi}) \begin{bmatrix} \mathbf{M}_s + \mathbf{R}_d m_d \mathbf{R}_d^T \\ m_d \mathbf{R}_d^T \end{bmatrix} \mathbf{R}_s \end{bmatrix}$$

$$\mathbf{C}_s(\boldsymbol{\varphi}) = \begin{bmatrix} \mathbf{T}_s & \mathbf{0}_{n\mathrm{x}(n+2)} \\ -\begin{bmatrix} \mathbf{I}_n & \mathbf{0}_{n\mathrm{x}1} \end{bmatrix} \mathbf{M}_t^{-1}(\boldsymbol{\varphi}) \left[\begin{bmatrix} \mathbf{K}_s & \mathbf{0}_{n\mathrm{x}1} \\ \mathbf{0}_{1\mathrm{x}n} & k_d \end{bmatrix} \begin{bmatrix} \mathbf{C}_s & \mathbf{0}_{n\mathrm{x}1} \\ \mathbf{0}_{1\mathrm{x}n} & c_d \end{bmatrix} \right] \\ \mathbf{0}_{1\mathrm{x}n} \quad 1 \quad \mathbf{0}_{1\mathrm{x}(n+1)} \\ -b\begin{bmatrix} \mathbf{R}_c^T & 1 \end{bmatrix} \mathbf{M}_t^{-1}(\boldsymbol{\varphi}) \left[\begin{bmatrix} \mathbf{K}_s & \mathbf{0}_{n\mathrm{x}1} \\ \mathbf{0}_{1\mathrm{x}n} & k_d \end{bmatrix} \begin{bmatrix} \mathbf{C}_s & \mathbf{0}_{n\mathrm{x}1} \\ \mathbf{0}_{1\mathrm{x}n} & c_d \end{bmatrix} \right] \\ c_d \begin{bmatrix} \mathbf{0}_{1\mathrm{x}2n+1} & 1 \end{bmatrix} \end{bmatrix} = \begin{bmatrix} \mathbf{T}_s & \mathbf{0}_{n\mathrm{x}(n+2)} \\ \begin{bmatrix} \mathbf{0}_{n\mathrm{x}(n+1)} & \mathbf{I}_n & \mathbf{0}_{n\mathrm{x}1} \end{bmatrix} \mathbf{A}_s(\boldsymbol{\varphi}) \\ \mathbf{0}_{1\mathrm{x}n} \quad 1 \quad \mathbf{0}_{1\mathrm{x}(n+1)} \\ b\begin{bmatrix} \mathbf{R}_c^T & 1 \end{bmatrix} \begin{bmatrix} \mathbf{0}_{(n+1)\mathrm{x}(n+1)} & \mathbf{I}_{n+1} \end{bmatrix} \mathbf{A}_s(\boldsymbol{\varphi}) \\ c_d \begin{bmatrix} \mathbf{0}_{1\mathrm{x}2n+1} & 1 \end{bmatrix} \end{bmatrix} \tag{23}$$

In the above expressions, the output matrix $\mathbf{C}_s(\boldsymbol{\varphi})$ accounts for a performance (output) variables vector $\mathbf{z}$ that includes inter-storey drifts and absolute accelerations for all floors, the attached mass displacement, the inerter force and the damper (dashpot) force, respectively, as needed in the illustrative design example. Further, $\mathbf{I}_a$ is the identity matrix of dimension a, $\mathbf{0}_{axb}$ is the zero matrix of dimensions axb, $\mathbf{T}_s$ is a transformation matrix defining relative responses between consecutive floors (i.e., a square matrix with dimension n_s with 1 in the diagonal and -1 in the first off-diagonal), and the auxiliary matrix $\mathbf{M}_t$ reads as

$$\mathbf{M}_t(\boldsymbol{\varphi}, \boldsymbol{\theta}_s) = \begin{bmatrix} \mathbf{M}_s(\boldsymbol{\theta}_s) + \mathbf{R}_d m_d \mathbf{R}_d^T + \mathbf{R}_c b \mathbf{R}_c^T & m_d \mathbf{R}_d + b \mathbf{R}_c \\ m_d \mathbf{R}_d^T + b \mathbf{R}_c^T & m_d + b \end{bmatrix}. \tag{24}$$

Combining Equations (22) and (4) leads to the representation in Equation (5) where

$$\mathbf{x} = \begin{bmatrix} \mathbf{x}_{ss} \\ \mathbf{x}_q \end{bmatrix} \quad \mathbf{A}(\boldsymbol{\varphi}) = \begin{bmatrix} \mathbf{A}_s(\boldsymbol{\varphi}) & \mathbf{E}_s(\boldsymbol{\varphi}) \mathbf{C}_q \\ \mathbf{0}_{n_q \mathrm{x}(2n+2)} & \mathbf{A}_q(\boldsymbol{\varphi}) \end{bmatrix} \quad \mathbf{E} = \begin{bmatrix} \mathbf{0}_{2(n+1)\mathrm{x}1} \\ \mathbf{E}_q \end{bmatrix} \quad \mathbf{C}(\boldsymbol{\varphi}) = \begin{bmatrix} \mathbf{C}_s(\boldsymbol{\varphi}) & \mathbf{0}_{n_z \mathrm{x} n_q} \end{bmatrix} \tag{25}$$

Lastly, the state-space matrices of the excitation model assumed in the design example, given by Equation (21), read as

$$\mathbf{A}_q = \begin{bmatrix} 0 & 1 & 0 & 0 \\ -\omega_g^2 & -2\zeta_g \omega_g & 0 & 0 \\ 0 & 0 & 0 & 1 \\ -\omega_g^2 & -2\zeta_g \omega_g & -\omega_f^2 & -2\zeta_f \omega_f \end{bmatrix} \quad \mathbf{E}_q = \begin{bmatrix} 0 \\ 1 \\ 0 \\ 0 \end{bmatrix}$$
$$\mathbf{C}_q = \sigma_o \begin{bmatrix} -\omega_g^2 & -2\zeta_g \omega_g & \omega_f^2 & 2\zeta_f \omega_f \end{bmatrix} \tag{26}$$

where σ_o is chosen such that the excitation has the desired a_{RMS} intensity.